

Aberrant hemichannel properties of Cx26 mutations causing skin disease and deafness

Dwan A. Gerido,^{1*} Adam M. DeRosa,^{2*} Gabriele Richard,³ and Thomas W. White^{1,2}

¹Department of Physiology and Biophysics and ²Graduate Program in Genetics, State University of New York, Stony Brook, New York; and ³GeneDx Incorporated, Gaithersburg, Maryland

Submitted 19 December 2006; accepted in final form 15 April 2007

Gerido DA, DeRosa AM, Richard G, White TW. Aberrant hemichannel properties of Cx26 mutations causing skin disease and deafness. *Am J Physiol Cell Physiol* 293: C337–C345, 2007. First published April 11, 2006; doi:10.1152/ajpcell.00626.2006.—Mutations in the human GJB2 gene, which encodes connexin26 (Cx26), underlie various forms of hereditary deafness and skin disease. While it has proven difficult to discern the exact pathological mechanisms that cause these disorders, studies have shown that the loss or abnormal function of Cx26 protein has a profound effect on tissue homeostasis. Here, we used the *Xenopus* oocyte expression system to examine the functional characteristics of a Cx26 mutation (G45E) that results in keratitis-ichthyosis-deafness syndrome (KIDS) with a fatal outcome. Our data showed that oocytes were able to express both wild-type Cx26 and its G45E variant, each of which formed hemichannels and gap junction channels. However, Cx26-G45E hemichannels displayed significantly greater whole cell currents than wild-type Cx26, leading to cell lysis and death. This severe phenotype could be rescued in the presence of elevated Ca²⁺ levels in the extracellular milieu. Cx26-G45E could also form intercellular channels with a similar efficiency as wild-type Cx26, however, with increased voltage sensitive gating. We also compared Cx26-G45E with a previously described Cx26 mutant, A40V, which has an overlapping human phenotype. We found that both dominant Cx26 mutants elicited similar functional consequences and that cells coexpressing mutant and wild-type connexins predominantly displayed mutant-like behavior. These data suggest that mutant hemichannels may act on cellular homeostasis in a manner that can be detrimental to the tissues in which they are expressed.

connexin

CONNEXINS have been implicated in a variety of hereditary human diseases including deafness and skin disease (1, 42, 44). The most common connexin-related disease is genetic deafness [sensorineural hearing loss (SNHL)], which can be nonsyndromic or syndromic when associated with skin disorders and other ectodermal abnormalities, such as palmoplantar keratoderma, Vohwinkel syndrome, Bart-Pumphrey syndrome, or keratitis-ichthyosis-deafness syndrome (KIDS) (13, 30). In most cases, SNHL is due to a mutation in the GJB2 gene that encodes connexin26 (Cx26), although mutations in other connexins also have been described (27). Functional analyses of specific Cx26 mutations associated with syndromic and nonsyndromic SNHL have been conducted to decipher the molecular mechanisms underlying these different disorders. Autosomal recessive hearing loss without skin involvement (nonsyndromic) is often due to a simple loss of channel function

altering cochlear intercellular communication (5, 43, 46). The lack of skin involvement in these cases suggests that loss of Cx26 function alone is not detrimental for the development and function of the epidermis. Thus, it has been hypothesized that mutant connexins resulting in syndromic SNHL associated with skin disorders must acquire novel activities compared with wild-type Cx26 channels to alter the epidermal differentiation.

Connexins are the basic subunits of a gap junction channels and consists of four membrane-spanning domains with two extracellular loops and cytoplasmic NH₂ and COOH termini. Six connexins oligomerize within the cell membrane to form a hemichannel, or one-half of an intercellular channel. A complete gap junction channel arises from the alignment of two hemichannels from adjacent cells in the extracellular space, creating a direct communication pathway between cytoplasm of neighboring cells (18). It was once believed that hemichannels must remained in a closed state until they were aligned with another hemichannel from an adjacent cell, but recent studies (16, 35) have suggested that hemichannels may play important roles in maintaining homeostasis under different physiological conditions.

If hemichannels play a role in normal physiology, it is possible that some connexin mutations may result in abnormal hemichannel activity that could contribute to disease pathology. This idea has been supported by studies of connexin mutations causing syndromic deafness associated with skin disease. One recently described example is the A40V mutation of Cx26, which is linked to a severe form of KIDS (25). A40V is located within the first extracellular domain of Cx26, a region in which multiple Cx26 mutations linked to syndromic deafness have been found (29). Injection of A40V cRNA into *Xenopus* oocytes resulted in a disorganization of cell pigmentation followed by cell death. Moreover, the induction of large membrane currents not seen in wild-type Cx26-expressing oocytes suggested the presence of aberrant A40V hemichannel activity (25), leading the authors to conclude that constitutively active hemichannels could contribute to the pathophysiology of this mutation.

Functional evaluation of additional KIDS mutations in Cx26 would help determine if aberrant hemichannel activity is a general pathological mechanism for this syndromic disorder. Here, we report the functional characteristics of a Cx26 mutation (G45E) that was observed in two previously described infants with a rare fatal form of KIDS. The children harboring the G45E mutation in GJB2 had congenital deafness, hyper-

* D. A. Gerido and A. M. DeRosa contributed equally to this work.

Address for reprint requests and other correspondence: T. W. White, Dept. of Physiology and Biophysics, State Univ. of New York, T5-147, Basic Science Tower, Stony Brook, NY 11794-8661 (e-mail: thomas.white@sunysb.edu).

The costs of publication of this article were defrayed in part by the payment of page charges. The article must therefore be hereby marked "advertisement" in accordance with 18 U.S.C. Section 1734 solely to indicate this fact.

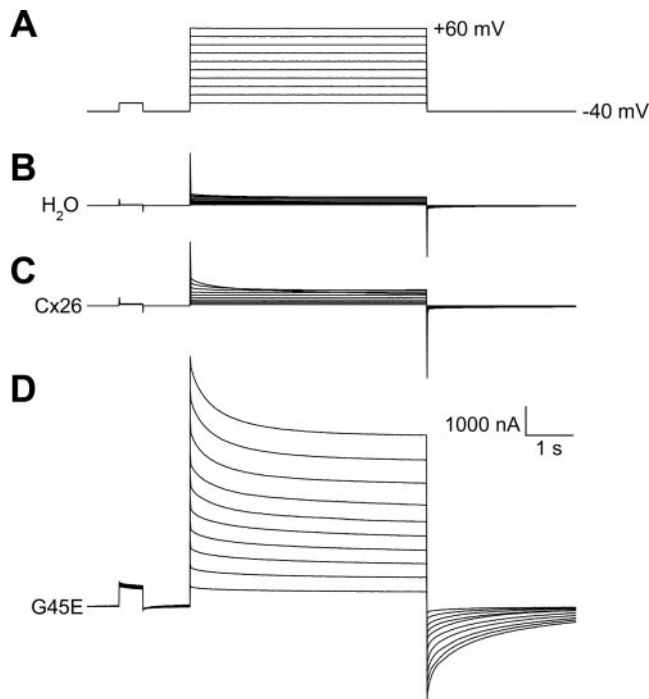


Fig. 1. Cx26-G45E induces large hemichannel currents in *Xenopus* oocytes. A: single cells were clamped at a holding potential of -40 mV and subjected to voltage pulses ranging from -30 to $+60$ mV in 10 -mV steps. B: H₂O-injected cells displayed negligible membrane currents. Connexin26 (Cx26; C) and G45E (D)-expressing oocytes exhibited hemichannel currents with G45E hemichannels displaying much larger currents at all tested voltages.

keratosis of the skin, and recurrent severe skin infections, which eventually lead to septicemia and death within the first year of life (14, 17, 21). Using an *in vitro* expression assay, we show that Cx26-G45E hemichannels display a significant increase in membrane current flow that results in cell death.

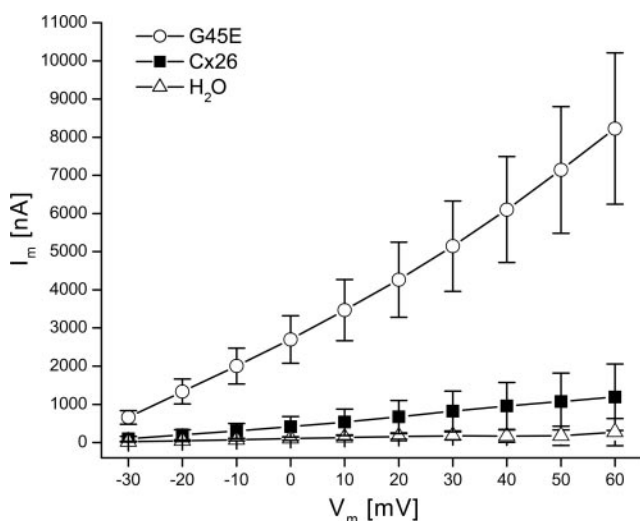


Fig. 2. Current-voltage relationships in control, Cx26, and Cx26-G45E oocytes. Steady-state currents (I_m) from each pulse were plotted as a function of membrane voltage (V_m). I_m s in H₂O-injected control cells ($n = 18$) were negligible at all V_m s. Cx26 currents ($n = 24$) were similar to those observed in control cells at lower voltages but increased at higher V_m . G45E cells ($n = 21$) exhibited significantly increased I_m s compared with either control or Cx26 oocytes. Data are means \pm SD.

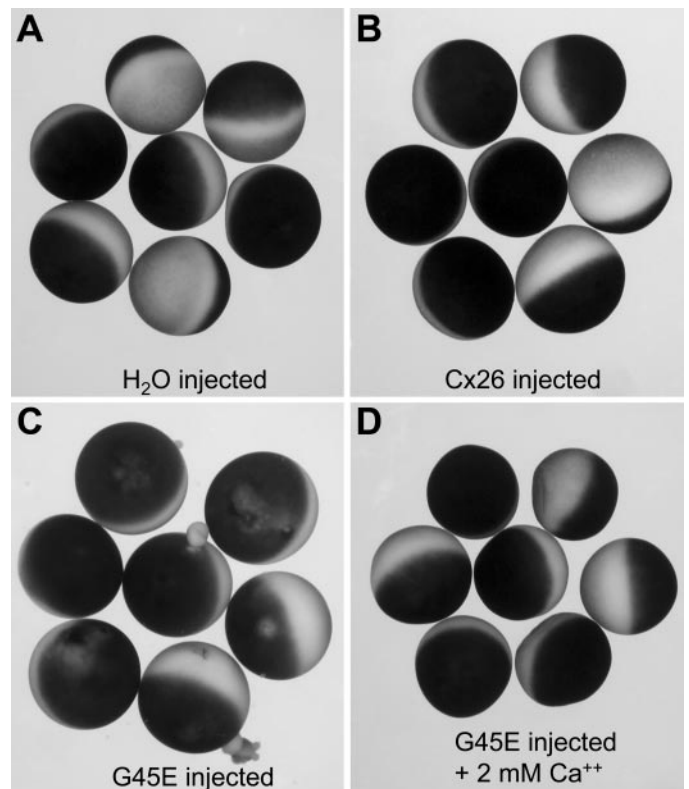


Fig. 3. Cx26-G45E hemichannels cause cell death that can be rescued by increased extracellular Ca^{2+} . Control, Cx26-injected, and G45E-injected cells were incubated in the presence or absence of 2 mM extracellular Ca^{2+} . H₂O (A)- and Cx26 (B)-injected cells survived in Ca^{2+} -free media, whereas G45E-injected cells (C) displayed increased pigment disorganization and blebbing at 8 h postinjection followed by cell lysis shortly thereafter. Incubation of G45E-injected oocytes in 2 mM Ca^{2+} (D) suppressed cell lysis and death.

Elevated Cx26-G45E hemichannel currents can be attenuated by increased extracellular Ca^{2+} levels that prevent cell death. Moreover, when oocytes are cultured in high Ca^{2+} , we demonstrate that Cx26-G45E can assemble into functional intercellular channels with coupling levels identical to those observed for Cx26. While the intercellular conductance was nearly identical, the voltage gating properties of Cx26-G45E and wild-type Cx26 gap junction channels displayed significant differences, further indicating a fundamental change in channel gating due to this mutation.

MATERIALS AND METHODS

Molecular cloning. Human wild-type Cx26 was cloned into the *Bam*HI restriction site of the pCS2+ expression vector for functional experiments in *Xenopus laevis* oocytes. Mutant Cx26-G45E was prepared by site-directed mutagenesis. Wild-type Cx26 was amplified by PCR using primers 5'-TGT TGT GGA TCC ATG GAT TGG GGC ACG CTG CAG ACG-3' and 3'-CTG CTC ATC TTC CCA CAC CTC CTT TGC-5' as well as 5'-AAG GAG GTG TGG GAA GAT GAG CAG GCC GAC-3' and 3'-TGT TGT GGA TCC TTA AAC TGG CTT TTT TGA CTT CCC AGA-5' and gene splicing by the overlap extension method (20) to create the glycine to glutamic acid substitution. Following amplification, G45E was initially cloned into pBlueScript and sequenced on both strands prior to being subcloned into the pCS2+ expression vector for *Xenopus laevis* expression experiments. Mutant Cx26-A40V was directly amplified from patient genomic DNA as previously described (25).

In vitro transcription, oocyte microinjection, and pairing. Human Cx26, A40V, and G45E were linearized using the *NotI* restriction site of pCS2+ and transcribed using the SP6 mMessage mMachine RNA protocol (Ambion, Austin, TX). Adult *Xenopus* females were anesthetized with ethyl-3-aminobenzoate methanesulfonate, and the ovarian lobes were surgically removed and digested for 1.5 h in a solution containing 50 mg/ml collagenase B and 50 mg/ml hyaluronidase in modified Barth's (MB) medium without Ca^{2+} . Stage V–VI oocytes were collected and injected first with 10 ng of antisense *Xenopus* Cx38 oligonucleotide to eliminate endogenous connexins (2, 4). The aforementioned antisense oligonucleotide-treated oocytes were then injected with wild-type Cx26, A40V, or G45E cRNA transcripts alone or a combination of wild-type and mutant Cx26 at a 1:1 ratio (total concentration of 5 ng/cell in all cases) or H_2O as a negative control. cRNA-injected oocytes were then cultured in Ca^{2+} -free MB medium or MB medium with elevated Ca^{2+} (2 mM CaCl_2). For measurements of gap junctional conductance, the vitelline envelopes were removed in a hypertonic solution (200 mM aspartic acid, 10 mM HEPES, 1 mM MgCl_2 , 10 mM EGTA, and 20 mM KCl; pH 7.4), and oocytes were manually paired with the vegetal poles apposed in MB medium with elevated Ca^{2+} .

Preparation of oocyte samples for Western blot analysis and quantification. Oocytes were collected in 1 ml of buffer containing 5 mM Tris (pH 8.0), 5 mM EDTA, and protease inhibitors and lysed using a series of mechanical passages through needles of diminishing caliber. Extracts were centrifuged at 1,000 *g* at 4°C for 5 min. The supernatant was then centrifuged at 100,000 *g* at 4°C for 30 min. Membrane pellets were resuspended in SDS sample buffer (2 μl /oocyte), and samples were separated on 15% SDS gels and transferred to nitrocellulose membranes. Blots were blocked with 5%

BSA in 1× PBS with 0.02% NaN_3 for 1 h and probed with a polyclonal Cx26 antibody at a 1:500 dilution (Zymed Laboratories, San Francisco, CA) followed by an incubation with alkaline phosphatase-conjugated anti-rabbit secondary antibody (Jackson ImmunoResearch Laboratories, West Grove, PA). Band intensities were quantified using Kodak 1D Image Analysis software (Eastman Kodak, Rochester, NY). Values from three independent experiments were normalized to the mean value of band intensity of the wild-type Cx26 sample.

Electrophysiological recording of hemichannel currents. Macroscopic recordings of hemichannel currents were recorded from single *Xenopus* oocytes using a GeneClamp 500 amplifier controlled by a personal computer (PC)-compatible computer through a Digidata 1320 interface (Axon Instruments, Foster City, CA). pCLAMP 8.0 software (Axon Instruments) was used to program stimulus and data collection paradigms. To obtain hemichannel current-voltage curves, cells were initially clamped at -40 mV and subjected to 5-s depolarizing voltage steps ranging from -30 to $+60$ mV in 10-mV increments. To test the effect of added Ca^{2+} on hemichannel currents, cells were transferred between 35-mm dishes containing MB media without Ca^{2+} or MB media supplemented with either 2 or 4 mM CaCl_2 . Hemichannel currents were recorded within 1–2 min of oocyte transfer.

Dual whole cell voltage clamp. Gap junctional coupling between oocyte pairs was measured using the dual whole cell voltage-clamp technique (36). Current and voltage electrodes (1.2 mm diameter, omega dot, Glass Company of America, Millville, NJ) were pulled to a resistance of 1–2 M Ω with a horizontal puller (Narishige, Tokyo, Japan) and filled with solution containing 3 M KCl, 10 mM EGTA, and 10 mM HEPES (pH 7.4). Voltage-clamp experiments were

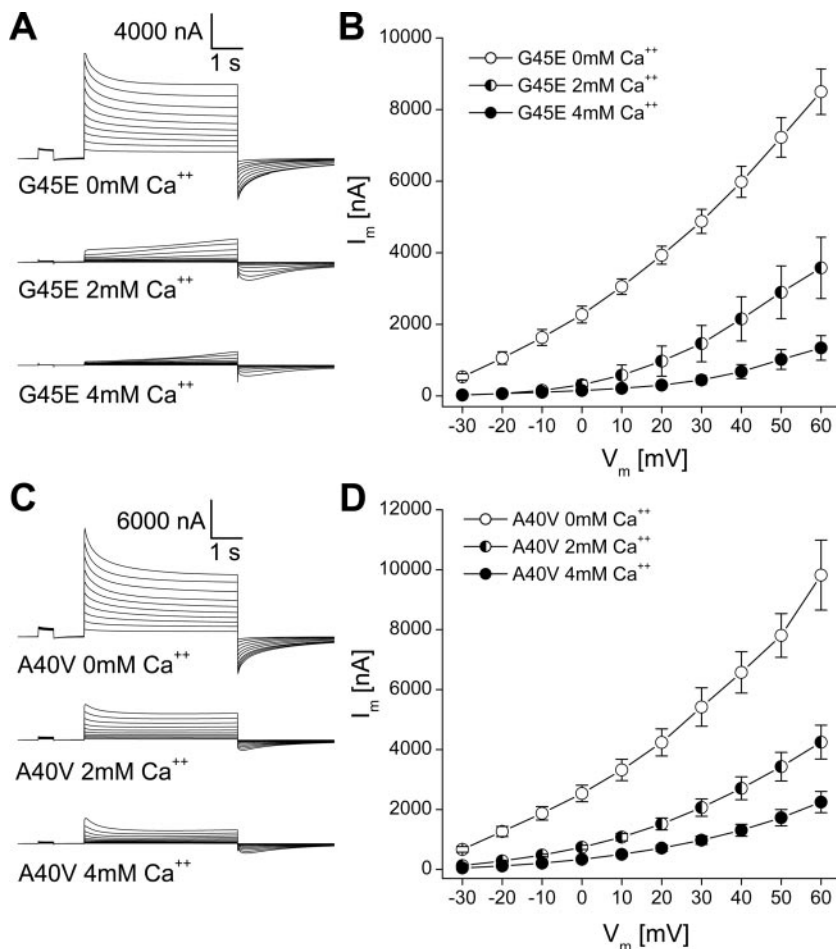


Fig. 4. Increased extracellular Ca^{2+} inhibits Cx26-G45E and CX26-A40V hemichannel currents. *A*: the large whole cell currents observed in G45E oocytes were suppressed by the addition of 2 and 4 mM Ca^{2+} to the medium. *B*: mean I_m s observed in G45E cells in the absence of Ca^{2+} were reduced in the presence of 2 and 4 mM Ca^{2+} ($n = 3-6$). *C*: similar to G45E-injected cells, A40V hemichannels displayed large I_m s that were suppressed by the addition of 2 and 4 mM Ca^{2+} . *D*: steady-state A40V currents exhibited a similar relationship to G45E cells with the addition of 2 and 4 mM Ca^{2+} ($n = 3-4$). Data are means \pm SE.

performed using two GeneClamp 500 amplifiers controlled by a PC-compatible computer through a Digidata 1320A interface (Axon Instruments).

For measurements of junctional conductance (G_j), both cells in a pair were initially clamped at -40 mV to eliminate any transjunctional potential (V_j). One cell was then subjected to alternating pulses of ± 20 mV while the current produced by the change in voltage was recorded in the second cell. The current delivered to the second cell was equal in magnitude to the junctional current (I_j), and G_j was calculated by dividing the measured current by the voltage difference as follows: $G_j = I_j / (V_1 - V_2)$, where V_1 and V_2 are the voltages in the first and second cells, respectively.

To determine voltage gating properties, V_j s of opposite polarity were generated by hyperpolarizing or depolarizing one cell in 20 mV steps (range = ± 120 mV) while clamping the second cell at -40 mV. Currents were measured at the end of the voltage pulse, at which time they approached steady state (I_{jss}). Macroscopic conductance (G_{jss}) was calculated by dividing I_{jss} by V_j (normalized to the values determined at ± 20 mV) and plotted against V_j . Data describing the relationship of G_{jss} as a function of V_j were analyzed using Origin 6.1 software (Microcal Software, Northampton, MA) and fit to a Boltzmann relation of the following form: $G_{jss} = (G_{jmax} - G_{jmin}) / \{1 + \exp[A(V_j - V_0)]\} + G_{jmin}$, where G_{jmax} (normalized to unity) is maximum conductance, G_{jmin} is the residual conductance at large values of V_j , and V_0 is the V_j at which $G_{jss} = (G_{jmax} - G_{jmin})/2$. The constant $A = nq/kT$ and represents the voltage sensitivity in terms of gating charge as the equivalent number (n) of electron charges (q) moving through the membrane, k is the Boltzmann constant, and T is the absolute temperature. To analyze channel closure kinetics, the initial 1,000 ms of current decay were plotted against time and fit to a monoexponential function to determine the time constant (τ) using Origin 6.1.

RESULTS

G45E induces gap junction hemichannel currents in single Xenopus oocytes. The G45E mutation in the GJB2 gene results in a single amino acid substitution in the first extracellular domain of Cx26 and causes KIDS, with a reported lethal outcome in two unrelated infants. To identify the functional consequences of mutation G45E, wild-type Cx26 and Cx26-G45E were expressed in *Xenopus* oocytes. Initially, single cells were subjected to depolarizing voltage pulses and membrane currents were recorded (Fig. 1). Control oocytes (H_2O injected) displayed negligible current flow over a range of voltages from -30 to $+60$ mV. Cx26-injected cells exhibited larger outward currents than control cells, confirming previous reports (15, 34) of low levels of hemichannel activity. In contrast, oocytes expressing the G45E mutation displayed currents of much greater magnitude in response to depolarization than either control or Cx26-injected cells. Thus, expression of G45E correlated with a markedly decreased plasma membrane electrical resistance, suggesting that G45E formed hemichannels that were functionally distinct from wild-type Cx26.

To quantitatively compare hemichannel currents produced by G45E and Cx26, mean I_{mss} values were plotted as a function of membrane potential (Fig. 2). Control oocytes displayed small currents at all voltages tested. Cx26-injected cells were initially indistinguishable from controls but showed greater current magnitudes at higher voltages with a maximum current approximately fourfold higher than control at the largest voltage tested ($+60$ mV, $P < 0.05$ by Student's t -test). G45E-expressing oocytes had much greater membrane currents than either H_2O - or Cx26-injected cells at all tested voltages. At

$+60$ mV, the G45E membrane current was 30-fold higher than control cells and more than 7-fold greater than Cx26-injected cells ($P < 0.05$). This statistically significant increase in membrane current may result from G45E forming hemichannels that are either fixed in the open configuration or gate open more easily than wild-type Cx26, leading to much greater ionic flux.

G45E induces cell death that can be rescued by elevated extracellular Ca^{2+} levels. We (25) have previously shown that another dominant Cx26 mutation associated with KIDS and the follicular occlusion triad (A40V) produced abnormal hemichannel currents when expressed in *Xenopus* oocytes and eventually led to lysis and death of the injected cells. Numerous studies (9, 28) have shown that increased extracellular Ca^{2+} suppresses gap junction hemichannel activity. Hence, if *Xenopus* oocytes expressing Cx26 mutants A40V and G45E die as result of abnormal hemichannel activity, this outcome may be prevented in the presence of increased Ca^{2+} levels. To test if Cx26-G45E indeed can affect cell viability in a Ca^{2+} -dependent manner, oocytes were cultured in medium in the presence or absence of Ca^{2+} (Fig. 3). Control and Cx26-expressing oocytes remained healthy as indicated by visual inspection when incubated in MB medium without Ca^{2+} (Fig. 3, A and B). In contrast, cells injected with G45E displayed pigment disorganization and blebbing of the ooplasm into the culture medium within 8 h (Fig. 3C), which preceded lysis and cell death within 12–24 h. Incubation of G45E-injected cells in MB media supplemented with ≥ 2 mM extracellular Ca^{2+} rescued this phenotype and preserved cell viability (Fig. 3D). These data suggested that the increased Ca^{2+} level suppressed G45E hemichannels and maintained cell viability.

If the addition of Ca^{2+} preserved cell viability by suppressing hemichannel activity, then whole cell membrane currents should be greatly reduced in elevated Ca^{2+} . To test this idea, we measured hemichannel currents from G45E- and A40V-

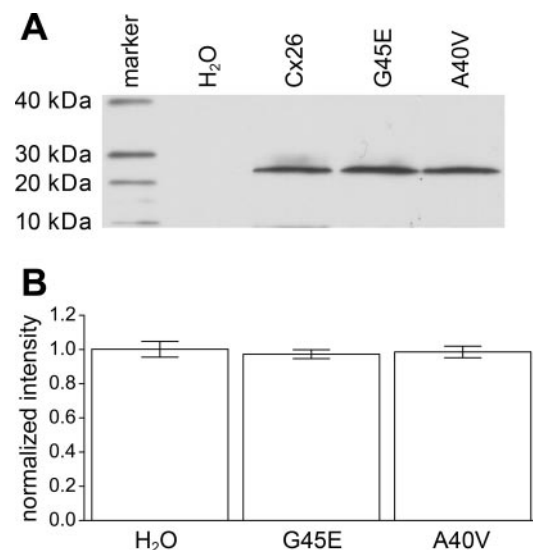


Fig. 5. Wild-type and mutant connexins are equally expressed in *Xenopus* oocytes. *A*: equal amounts of membrane extracts were probed with antibodies for Cx26. H_2O -injected controls did not express Cx26, as expected. Cx26, G45E, and A40V were readily detected in lanes corresponding to each injection condition. *B*: quantitation of Cx26 expression by densitometry revealed that Cx26, G45E, and A40V were expressed in equal amounts ($n = 3$). Data are means \pm SD.

expressing cells in media containing 0, 2, or 4 mM Ca^{2+} (Fig. 4). Oocytes expressing G45E in the absence of extracellular Ca^{2+} produced large outward currents that were reduced by 2 mM Ca^{2+} and further reduced by 4 mM Ca^{2+} (Fig. 4A). To quantitate these findings, I_{mss} values of G45E oocytes in the presence and absence of Ca^{2+} were plotted as a function of voltage. The addition of 2 and 4 mM Ca^{2+} produced a significant decrease in current flow at all tested voltages, with the maximum voltage displaying a greater than twofold decrease at 2 mM Ca^{2+} and a sixfold decrease in hemichannel current in 4 mM Ca^{2+} . In addition, the threshold of voltage activation was shifted to more positive potentials with increased Ca^{2+} concentration (Fig. 4B).

Like G45E, the A40V Cx26 mutation has been previously shown to induce hemichannel-mediated cell lysis and death (25); however, the ability of elevated Ca^{2+} to rescue A40V had not been tested. To determine whether elevated Ca^{2+} could also suppress A40V activity, we measured membrane currents from A40V hemichannels in the presence and absence of elevated extracellular Ca^{2+} . In the absence of Ca^{2+} , A40V-injected oocytes produced large currents similar to those observed in G45E cells (Fig. 4C). The addition of Ca^{2+} to the media produced a dramatic reduction in hemichannel current flow consistent with the results observed in G45E cells. Again, quantitation of I_{mss} values revealed a significant decrease in hemichannel activity in the presence of Ca^{2+} and a positive shift in the threshold of voltage activation (Fig. 4D). This

decrease in current flow was detected at all voltages tested, with the maximum decline being twofold in 2 mM Ca^{2+} and fourfold in 4 mM Ca^{2+} at +60 mV. Taken together, these data indicate a significant reduction in the number of active hemichannels with the elevation of extracellular Ca^{2+} for both G45E and A40V and that these two mutations share similar functional properties.

G45E and A40V may contribute to cellular pathology through abnormal hemichannel activity; however, wild-type Cx26 also induced low levels of hemichannel current, and the differences in current magnitude between the wild type and mutants could have resulted from different levels of protein expression in each condition. To examine the levels of connexin protein expressed in oocytes, we performed Western blot analysis with cell extracts from control (H_2O injected) and Cx26-, G45E-, and A40V-injected cells (Fig. 5). Antibodies for Cx26 failed to detect protein expression in control cells but readily detected expression of Cx26, G45E, and A40V following injection of their respective cRNAs (Fig. 5A). To quantify expression levels, we measured the band intensities of G45E and A40V and compared them to the value obtained for Cx26 (Fig. 5B). Cx26, G45E, and A40V were all expressed in equal amounts, and thus the differences in hemichannel current magnitude were not due to the relative overexpression of mutant protein.

Previous reports have described the G45E mutation as dominant in the Caucasian population; however, this mutation has

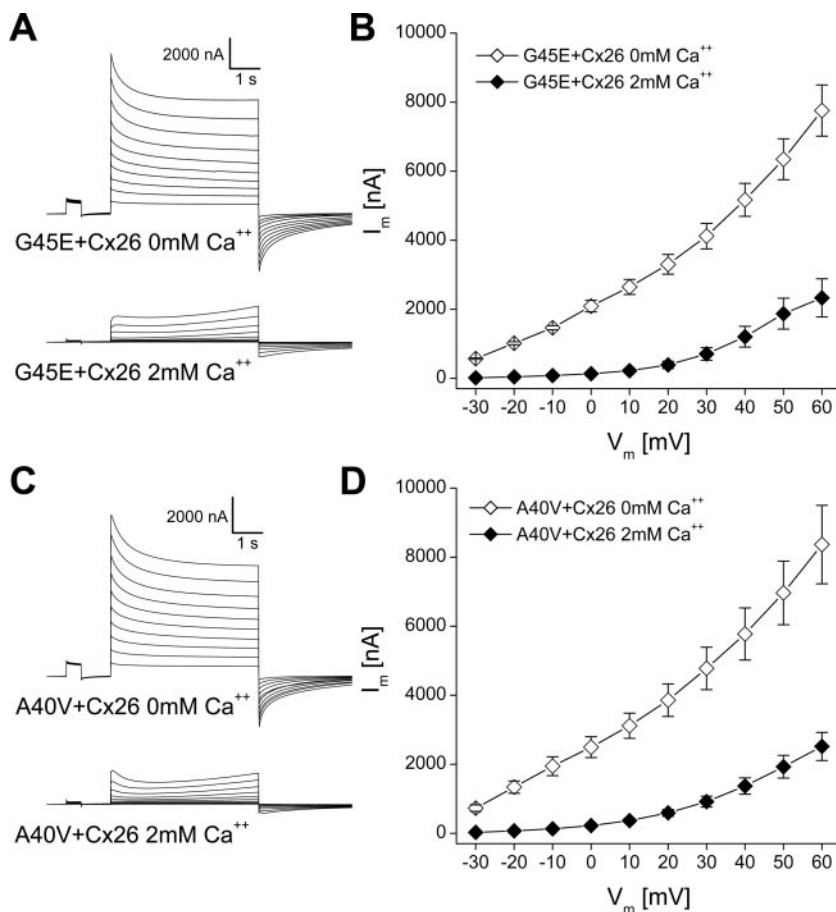


Fig. 6. Cx26-G45E and Cx26-A40V exhibit dominant behavior in single *Xenopus* oocytes. *A*: oocytes coinjected with wild-type Cx26 and G45E displayed large I_{mss} that were suppressed in the presence of 2 mM Ca^{2+} . *B*: mean I_{mss} were elevated in coinjected cells without extracellular Ca^{2+} but were reduced when cells were incubated in media containing 2 mM Ca^{2+} ($n = 3-8$). *C*: cells coinjected with A40V and wild-type Cx26 also exhibited large I_{mss} in the absence of Ca^{2+} that were suppressed when cells were transferred to media containing 2 mM Ca^{2+} . *D*: mean I_{mss} for A40V-coinjected oocytes were also significantly reduced by 2 mM Ca^{2+} ($n = 4$). Data are means \pm SE.

also been linked to recessive deafness in some Asian populations (26). Given the conflicting nature of these data, we performed experiments to examine the impact of the mutant allele on wild-type Cx26 function. To test for dominant activity, we injected oocytes with both wild-type Cx26 and G45E in a 1:1 ratio and measured hemichannel currents in the absence and presence of elevated extracellular Ca^{2+} . Oocytes coexpressing G45E and wild-type Cx26 displayed large membrane currents similar to those observed with expression of G45E alone (Fig. 6A). The large membrane currents seen in coinjected oocytes were reduced with the addition of 2 mM Ca^{2+} in a manner also consistent with the results from cells only expressing the G45E variant of Cx26. Quantitation of I_{mss} values revealed a significant decrease in membrane current with the addition of Ca^{2+} , displaying a threefold decrease at the maximum voltage tested (Fig. 6B).

Given that oocytes injected with A40V exhibited properties similar to G45E, we also examined the dominance of A40V by coinjecting cells with A40V and wild-type Cx26. Oocytes expressing A40V in conjunction with wild-type Cx26 again displayed large membrane currents that were reduced by the addition of 2 mM Ca^{2+} (Fig. 6C). Again, quantitation revealed a significant decrease with the addition of calcium with a threefold difference at a membrane potential of +60 mV (Fig. 6D). Together, these data show that both G45E and A40V exhibited dominant, Ca^{2+} -sensitive hemichannel activity when coexpressed with wild-type Cx26.

G45E also forms gap junction channels in paired Xenopus oocytes. We and others (5–7, 24, 38, 41, 45) have previously shown that not all disease-causing mutations in Cx26 result in the complete loss of gap junction channel activity. The ability to rescue viability in cells expressing G45E with elevated extracellular Ca^{2+} allowed us to examine its ability to form intercellular channels using the dual cell voltage-clamp technique in paired oocytes (Fig. 7). After G45E or Cx26 cRNA

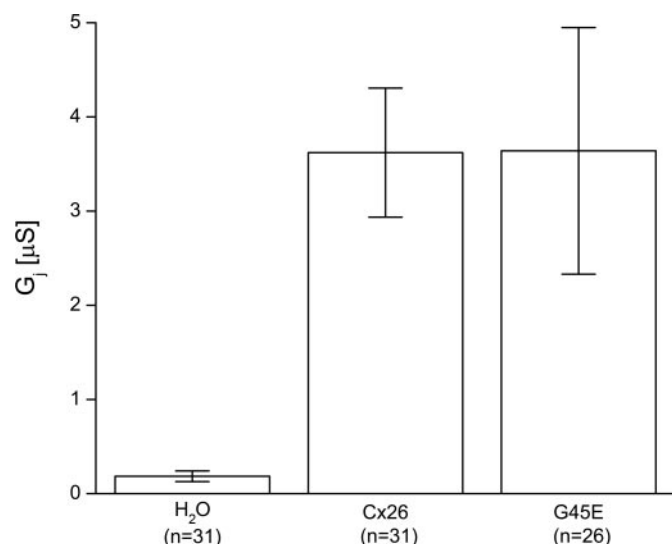


Fig. 7. Cx26-G45E forms gap junction channels in paired oocytes. Junctional conductance (G_j) was measured in oocyte pairs injected with Cx26, G45E, or H₂O. Cells were incubated in 2 mM Ca^{2+} to inhibit hemichannel activity. Cx26 ($n = 31$) and G45E ($n = 26$) pairs displayed a 20-fold increase in conductance compared with H₂O ($n = 31$)-injected controls. There was no difference in the level of coupling between Cx26 and G45E channels. Data are means \pm SD.

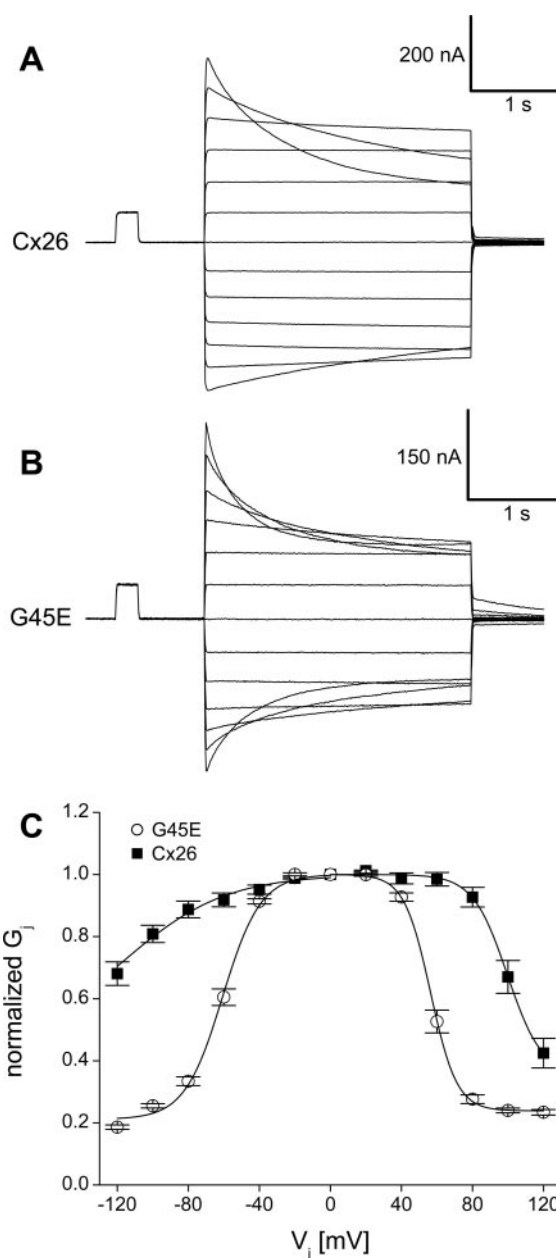


Fig. 8. Cx26-G45E gap junctions have increased voltage sensitivity. Junctional currents (I_j) induced by transjunctional voltages (V_j s) were plotted as a function of time. A: Cx26 gap junction channels were weakly voltage gated, exhibiting an asymmetric pattern of current decay at V_j s $> \pm 80$ mV that had more complete closure and faster kinetics for depolarization than hyperpolarization. B: G45E gap junction channels were more voltage sensitive than those of Cx26, showing current decay at lower V_j values (greater than ± 40 mV) that was also more symmetrical for voltages of either polarity. C: equilibrium gating properties were analyzed by plotting normalized steady-state G_j against V_j and fitting to the Boltzmann equation. G45E gap junction channels displayed a more symmetric gating than Cx26 channels at much lower V_j s. Boltzmann parameters are shown in Table 1. Data are means \pm SE.

injection, oocytes were paired and incubated in medium with 2 mM Ca^{2+} . H₂O-injected cells were used as negative controls. Wild-type Cx26 formed functional channels with G_j that was 20-fold higher than background levels recorded in control pairs. Oocyte pairs injected with G45E also had a mean conductance 20-fold higher than the background level and

indistinguishable from wild-type Cx26 ($P > 0.05$). Thus, the G45E mutation retained the ability to form functional gap junction channels when hemichannel activity was suppressed by elevated extracellular Ca^{2+} .

G45E intercellular channels have altered voltage gating properties. The ability of G45E to form functional gap junction channels in elevated extracellular Ca^{2+} allowed its voltage gating properties to be compared with wild-type Cx26 channels. Although the macroscopic conductance measurements were indistinguishable, we found that the voltage gating properties of Cx26 and G45E channels were markedly different. Figure 8 shows the gap junctional currents (I_j) for wild-type Cx26 and G45E recorded for a series of different V_j s. Cx26 currents were consistent with previous data showing an asymmetric decay at higher voltages with greater closure for positive V_j s (Fig. 8A) (2, 24). In contrast, G45E gap junctions exhibited a more symmetric current decline in response to V_j s of either polarity (Fig. 8B). In addition to the increased symmetry, G45E currents decayed more rapidly than wild-type Cx26. For example, at $V_j = -120$ mV, G45E currents decayed with a mean τ value of 0.19 ± 0.05 s ($n = 6$), whereas Cx26 currents decayed six times slower with a mean τ value of 1.15 ± 0.38 s ($P < 0.05$, $n = 5$).

To analyze the equilibrium voltage gating properties, G_{jss} values were normalized, plotted against V_j , and fitted to a Boltzmann equation (Fig. 8C). This analysis revealed that for Cx26, V_0 (which corresponds to the midway point between G_{jmax} and G_{jmin}) was asymmetric with values of 99 and -117 mV for positive and negative V_j s, respectively (Table 1). Conversely, V_0 values for G45E channels were more symmetrical and much lower, with positive and negative V_0 values of $+56$ and -61 mV. These data demonstrate that, in addition to increased hemichannel function, the magnitude and kinetics of the voltage gating properties of gap junction channels made from G45E differed quantitatively from those of wild-type Cx26.

We also tested for a dominant impact of G45E on wild-type Cx26 in gap junction channels between paired oocytes (Fig. 9). Cell pairs coinjected with equal amounts of wild-type Cx26 and G45E cRNA were able to form functional gap junctions that exhibited significantly increased conductance compared with H_2O -injected negative controls (Fig. 9A) but were not statistically different from the coupling levels in oocyte pairs injected with Cx26 or G45E alone (see Fig. 7). An examination of the voltage-induced current decay revealed that coinjected

Table 1. Boltzmann parameters for wild-type Cx26 and G45E mutant channels

Cell Injection	V_j	V_0	G_{jmin}	A
Cx26	+	99	0.35	0.10
Cx26	-	-117	0.44	0.03
G45E	+	56	0.23	0.14
G45E	-	-61	0.21	0.09
Cx26 + G45E	+	61	0.24	0.10
Cx26 + G45E	-	-63	0.21	0.07

V_j is the transjunctional membrane potential, with + and - indicating polarity. V_0 indicates the voltage measured midway through the junctional conductance decline, G_{jmin} represents the minimum junctional conductance value, and A denotes the cooperativity constant, which reflects the number of charges moving through the transjunctional field. Cx26, connexin26.

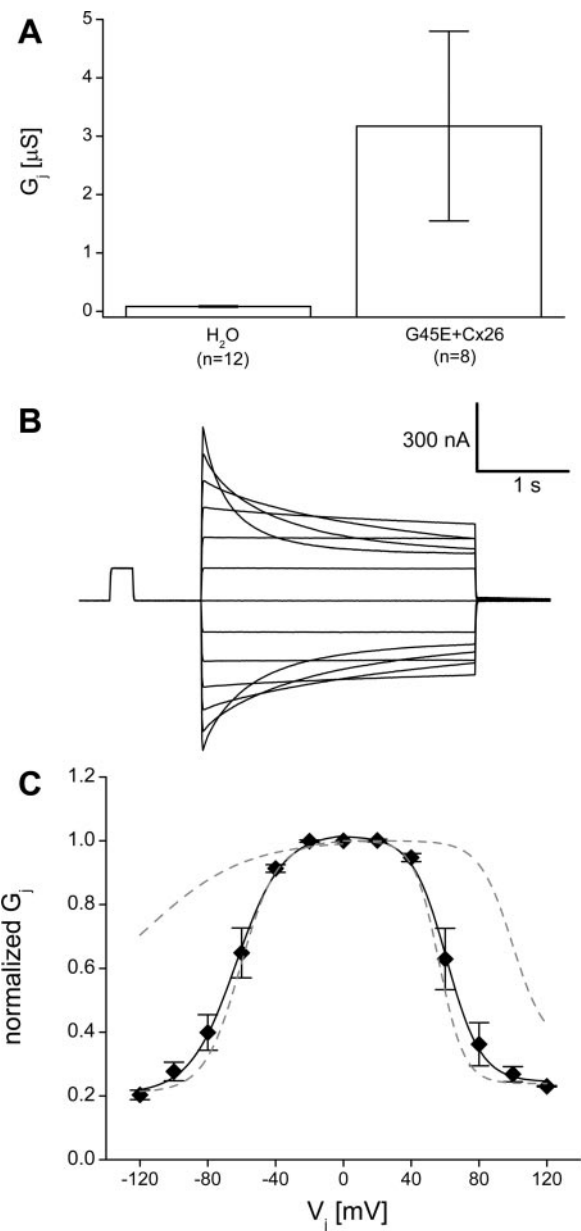


Fig. 9. Coinjected wild-type Cx26 and G45E form intercellular channels dominated by G45E gating properties. G_j was measured in oocyte pairs coinjected with equal amounts of wild-type Cx26 and G45E cRNA and incubated in 2 mM Ca^{2+} to prevent cell death. A: compared with H_2O -injected controls, coinjected cells displayed a 50-fold increase in G_j . B: I_j s induced by changes in V_j were plotted as a function of time and analyzed for voltage gating sensitivity. Coinjected channels were more voltage sensitive compared with Cx26 channels alone, exhibiting a pattern similar to that observed in G45E gap junction channels. C: equilibrium gating properties were analyzed by plotting normalized steady-state G_j against V_j and fitting to the Boltzmann equation. Dashed lines are Boltzmann fits of homomeric Cx26 and G45E taken from Fig. 8. The equilibrium gating properties revealed that coinjected cells exhibited more symmetric gating than Cx26 and behaved similarly to G45E expressed alone. Boltzmann parameters are shown in Table 1. Data are means \pm SE.

pairs displayed voltage gating properties more like those of gap junctions composed of G45E alone rather than Cx26 alone. Specifically, the voltage sensitivity of the currents was more symmetrical than Cx26 with faster gating kinetics (Fig. 9B). Analysis of the equilibrium voltage gating properties con-

firmed that coinjected cell pairs were dominated by G45E-like behavior (Fig. 9C). The equilibrium properties of cell pairs coexpressing G45E and Cx26 were deduced from a Boltzmann fit and found to be nearly identical to those of pairs injected with G45E alone (Table 1). These data showed that the voltage gating properties of gap junction channels made from an equal mixture of Cx26 and G45E did not differ markedly from those composed of G45E alone and suggested that G45E exerted a dominant gating phenotype on wild-type Cx26.

DISCUSSION

Numerous studies have linked mutations in the GJB2 gene to syndromic deafness associated with skin disease. In the case of KIDS, all pathogenic mutations cluster in regions coding for the first extracellular domain and the NH₂-terminal of Cx26, implying common functional defects. In the present study, we showed that the G45E and A40V mutant forms of Cx26 produced greatly increased hemichannel activity that ultimately led to cell death. This severe phenotype could be rescued by elevated extracellular Ca²⁺, which allowed Cx26-G45E intercellular channels to be evaluated. G45E mutant gap junction channels also displayed significantly altered voltage-sensitive gating. These findings are consistent with the hypothesis that aberrant hemichannel activity might be a common feature of some KIDS mutations and may contribute to severe epidermal pathology in these cases.

While the rare fatal form of KIDS has been associated with Cx26-G45E in two unrelated Caucasian patients (14, 17, 21), it has also been linked to recessive nonsyndromic deafness in some Asian populations. In a large study of Japanese patients with nonsyndromic SNHL, G45E was detected in 16% of the GJB2 disease alleles (26). Among Japanese patients, G45E was classified as a recessive allele as it was always present homozygously or as compound heterozygotes with other GJB2 mutations in deaf individuals. In addition, it was never detected in control individuals or classified as causing syndromic deafness associated with skin disease (12, 26).

Our data are consistent with a dominant gain of function for G45E, which rapidly killed *Xenopus* oocytes through aberrant hemichannel activity. Further support for the cellular lethality of Cx26-G45E comes from a report of hemichannel activity in transfected HEK-293 cells that appeared while this article was being written (37). Stong et al. (37) reported that Cx26-G45E expression facilitated dye uptake, resulting in apoptosis within 24 h of cell transfection, and cell death could be rescued by increasing the extracellular Ca²⁺ concentration. Thus, in two different functional expression systems, Cx26-G45E led to aberrant hemichannel formation and cell lysis, functional properties that we show were shared by a second severe KIDS mutation in GJB2, Cx26-A40V. To date, the A40V mutation has only been associated with KIDS and the follicular occlusion triad (25).

Nine connexin genes, including Cx26, are expressed during epidermal morphogenesis, and gap junctional communication plays an important role in keratinocyte growth and differentiation (8, 22). Mutations in Cx26 are the leading cause of hereditary deafness, which can be associated with a variety of skin diseases (23, 31–33, 40). The presence of Cx26 mutations in syndromic and nonsyndromic deafness suggests that different functional consequences of distinct mutations may corre-

spond to unique pathological states. For example, many non-syndromic mutations in the GJB2 gene have resulted in altered protein trafficking, loss of channel function, or alteration of channel permeability, without causing cell death (43, 46). In contrast, we and others (25, 37) have shown that two separate KIDS mutations exhibited lethal hemichannel activity that may have contributed to both hearing loss and the epidermal pathology. Further support for this aberrant hemichannel hypothesis comes from studies of mutations in the GJB6 gene (which encodes Cx30) causing hidrotic ectodermal dysplasia (HED). Two HED-associated Cx30 mutants, G11R and A88V, induced cell death in *Xenopus* oocytes, which could have resulted from the presence of functional hemichannels, an idea supported by the detection of large voltage-activated currents in single oocytes expressing mutant proteins that were not seen in cells injected with wild-type Cx30 (10). Furthermore, transfected cells expressing the mutant channels had a two- to threefold higher ATP leakage than control cells, suggesting that ATP release through unregulated hemichannels may play a role in the HED phenotype (10). In addition to causing cell depolarization and death, hemichannels could induce the release of metabolites into the extracellular space in the epidermis and influence the regulation of keratinocyte growth and differentiation.

Extracellular Ca²⁺ plays an important role in normal epidermal differentiation, regulating cell proliferation, terminal differentiation, and cell-to-cell adhesion. In addition, altered Ca²⁺ regulation has been implicated in the pathogenesis of some epidermal diseases (3, 11, 19, 39). An increase in the extracellular Ca²⁺ concentration is thought to drive the developmental switch from keratinocyte proliferation to terminal differentiation by providing a reservoir of Ca²⁺ that influences intracellular Ca²⁺-dependant signaling processes. However, it is not known if this developmentally regulated rise in extracellular Ca²⁺ achieves concentrations sufficiently high to inhibit G45E or A40V mutant hemichannels. While we have not tried other hemichannel blockers, future studies may identify novel treatment strategies seeking to modulate epidermal Ca²⁺ concentrations pharmacologically or seeking novel blocking agents that specifically act on Cx26 hemichannels.

ACKNOWLEDGMENTS

We thank Gülistan Meşe for critically reading the manuscript.

GRANTS

This work was supported by National Institutes of Health Grants DC-06652 and EY-13163 (to T. W. White).

REFERENCES

1. Anand RJ, Hackam DJ. The role of gap junctions in health and disease. *Crit Care Med* 33: S535–S538, 2005.
2. Barrio LC, Suchyna T, Bargiello T, Xu LX, Roginski RS, Bennett MV, Nicholson BJ. Gap junctions formed by connexins 26 and 32 alone and in combination are differently affected by applied voltage. *Proc Natl Acad Sci USA* 88: 8410–8414, 1991.
3. Bikle DD, Oda Y, Xie Z. Calcium and 1,25(OH)₂D: interacting drivers of epidermal differentiation. *J Steroid Biochem Mol Biol* 89–90: 355–360, 2004.
4. Bruzzone R, Haefliger JA, Gimlich RL, Paul DL. Connexin40, a component of gap junctions in vascular endothelium, is restricted in its ability to interact with other connexins. *Mol Biol Cell* 4: 7–20, 1993.
5. Bruzzone R, Veronesi V, Gomes D, Bicego M, Duval N, Marlin S, Petit C, D'Andrea P, White TW. Loss-of-function and residual channel

- activity of connexin26 mutations associated with non-syndromic deafness. *FEBS Lett* 533: 79–88, 2003.
6. **Choung YH, Moon SK, Park HJ.** Functional study of GJB2 in hereditary hearing loss. *Laryngoscope* 112: 1667–1671, 2002.
 7. **D'Andrea P, Veronesi V, Bicego M, Melchionda S, Zelante L, Di Iorio E, Bruzzone R, Gasparini P.** Hearing loss: frequency and functional studies of the most common connexin26 alleles. *Biochem Biophys Res Commun* 296: 685–691, 2002.
 8. **Di WL, Common JE, Kelsell DP.** Connexin 26 expression and mutation analysis in epidermal disease. *Cell Commun Adhes* 8: 415–418, 2001.
 9. **Ebihara L, Steiner E.** Properties of a nonjunctional current expressed from a rat connexin46 cDNA in *Xenopus* oocytes. *J Gen Physiol* 102: 59–74, 1993.
 10. **Essenfelder GM, Bruzzone R, Lamartine J, Charollais A, Blanchet-Bardon C, Barbe MT, Meda P, Waksman G.** Connexin30 mutations responsible for hidrotic ectodermal dysplasia cause abnormal hemichannel activity. *Hum Mol Genet* 13: 1703–1714, 2004.
 11. **Fairley JA.** Calcium metabolism and the pathogenesis of dermatologic disease. *Semin Dermatol* 10: 225–231, 1991.
 12. **Fuse Y, Doi K, Hasegawa T, Sugii A, Hibino H, Kubo T.** Three novel connexin26 gene mutations in autosomal recessive non-syndromic deafness. *Neuroreport* 10: 1853–1857, 1999.
 13. **Gerido DA, White TW.** Connexin disorders of the ear, skin, and lens. *Biochim Biophys Acta* 1662: 159–170, 2004.
 14. **Gilliam A, Williams ML.** Fatal septicemia in an infant with keratitis, ichthyosis, and deafness (KID) syndrome. *Pediatr Dermatol* 19: 232–236, 2002.
 15. **Gonzalez D, Gomez-Hernandez JM, Barrio LC.** Species specificity of mammalian connexin-26 to form open voltage-gated hemichannels. *FASEB J* 20: 2329–2338, 2006.
 16. **Goodenough DA, Paul DL.** Beyond the gap: functions of unpaired connexon channels. *Nat Rev Mol Cell Biol* 4: 285–294, 2003.
 17. **Griffith AJ, Yang Y, Pryor SP, Park HJ, Jabs EW, Nadol JB Jr, Russell LJ, Wasserman DI, Richard G, Adams JC, Merchant SN.** Cochleosaccular dysplasia associated with a connexin 26 mutation in keratitis-ichthyosis-deafness syndrome. *Laryngoscope* 116: 1404–1408, 2006.
 18. **Harris AL.** Emerging issues of connexin channels: biophysics fills the gap. *Q Rev Biophys* 34: 325–472, 2001.
 19. **Hennings H, Michael D, Cheng C, Steinert P, Holbrook K, Yuspa SH.** Calcium regulation of growth and differentiation of mouse epidermal cells in culture. *Cell* 19: 245–254, 1980.
 20. **Horton RM, Cai ZL, Ho SN, Pease LR.** Gene splicing by overlap extension: tailor-made genes using the polymerase chain reaction. *Bio-techniques* 8: 528–535, 1990.
 21. **Janecke AR, Hennies HC, Gunther B, Gansl G, Smolle J, Messmer EM, Utermann G, Rittinger O.** GJB2 mutations in keratitis-ichthyosis-deafness syndrome including its fatal form. *Am J Med Genet A* 133: 128–131, 2005.
 22. **Kelsell DP, Wilgoss AL, Richard G, Stevens HP, Munro CS, Leigh IM.** Connexin mutations associated with palmoplantar keratoderma and profound deafness in a single family. *Eur J Hum Genet* 8: 469–472, 2000.
 23. **Maestrini E, Korge BP, Ocana-Sierra J, Calzolari E, Cambiaghi S, Scudder PM, Hovnanian A, Monaco AP, Munro CS.** A missense mutation in connexin26, D66H, causes mutilating keratoderma with sensorineural deafness (Vohwinkel's syndrome) in three unrelated families. *Hum Mol Genet* 8: 1237–1243, 1999.
 24. **Mese G, Londin E, Mui R, Brink PR, White TW.** Altered gating properties of functional Cx26 mutants associated with recessive non-syndromic hearing loss. *Hum Genet* 115: 191–199, 2004.
 25. **Montgomery JR, White TW, Martin BL, Turner ML, Holland SM.** A novel connexin 26 gene mutation associated with features of the keratitis-ichthyosis-deafness syndrome and the follicular occlusion triad. *J Am Acad Dermatol* 51: 377–382, 2004.
 26. **Ohtsuka A, Yuge I, Kimura S, Namba A, Abe S, Van Laer L, Van Camp G, Usami S.** GJB2 deafness gene shows a specific spectrum of mutations in Japan, including a frequent founder mutation. *Hum Genet* 112: 329–333, 2003.
 27. **Petit C.** From deafness genes to hearing mechanisms: harmony and counterpoint. *Trends Mol Med* 12: 57–64, 2006.
 28. **Pfahnl A, Dahl G.** Gating of cx46 gap junction hemichannels by calcium and voltage. *Pflügers Arch* 437: 345–353, 1999.
 29. **Richard G.** Connexins: a connection with the skin. *Exp Dermatol* 9: 77–96, 2000.
 30. **Richard G.** Connexin disorders of the skin. *Clin Dermatol* 23: 23–32, 2005.
 31. **Richard G, Brown N, Ishida-Yamamoto A, Krol A.** Expanding the phenotypic spectrum of Cx26 disorders: Bart-Pumphrey syndrome is caused by a novel missense mutation in GJB2. *J Invest Dermatol* 123: 856–863, 2004.
 32. **Richard G, Rouan F, Willoughby CE, Brown N, Chung P, Ryynanen M, Jabs EW, Bale SJ, DiGiovanna JJ, Uitto J, Russell L.** Missense mutations in GJB2 encoding connexin-26 cause the ectodermal dysplasia keratitis-ichthyosis-deafness syndrome. *Am J Hum Genet* 70: 1341–1348, 2002.
 33. **Richard G, White TW, Smith LE, Bailey RA, Compton JG, Paul DL, Bale SJ.** Functional defects of Cx26 resulting from a heterozygous missense mutation in a family with dominant deaf-mutism and palmoplantar keratoderma. *Hum Genet* 103: 393–399, 1998.
 34. **Ripps H, Qian H, Zakevicius J.** Properties of connexin26 hemichannels expressed in *Xenopus* oocytes. *Cell Mol Neurobiol* 24: 647–665, 2004.
 35. **Saez JC, Retamal MA, Basilio D, Bukauskas FF, Bennett MV.** Connexin-based gap junction hemichannels: gating mechanisms. *Biochim Biophys Acta* 1711: 215–224, 2005.
 36. **Spray DC, Harris AL, Bennett MV.** Equilibrium properties of a voltage-dependent junctional conductance. *J Gen Physiol* 77: 77–93, 1981.
 37. **Stong BC, Chang Q, Ahmad S, Lin X.** A novel mechanism for connexin 26 mutation linked deafness: cell death caused by leaky gap junction hemichannels. *Laryngoscope* 116: 2205–2210, 2006.
 38. **Thonnissen E, Rabionet R, Arbones ML, Estivill X, Willecke K, Ott T.** Human connexin26 (GJB2) deafness mutations affect the function of gap junction channels at different levels of protein expression. *Hum Genet* 111: 190–197, 2002.
 39. **Tu CL, Oda Y, Komuves L, Bikle DD.** The role of the calcium-sensing receptor in epidermal differentiation. *Cell Calcium* 35: 265–273, 2004.
 40. **van Steensel MA, van Geel M, Nahuys M, Smitt JH, Steijlen PM.** A novel connexin 26 mutation in a patient diagnosed with keratitis-ichthyosis-deafness syndrome. *J Invest Dermatol* 118: 724–727, 2002.
 41. **Wang HL, Chang WT, Li AH, Yeh TH, Wu CY, Chen MS, Huang PC.** Functional analysis of connexin-26 mutants associated with hereditary recessive deafness. *J Neurochem* 84: 735–742, 2003.
 42. **Wei CJ, Xu X, Lo CW.** Connexins and cell signaling in development and disease. *Annu Rev Cell Dev Biol* 20: 811–838, 2004.
 43. **White TW.** Functional analysis of human Cx26 mutations associated with deafness. *Brain Res Brain Res Rev* 32: 181–183, 2000.
 44. **White TW, Paul DL.** Genetic diseases and gene knockouts reveal diverse connexin functions. *Annu Rev Physiol* 61: 283–310, 1999.
 45. **Zhang Y, Tang W, Ahmad S, Sipp JA, Chen P, Lin X.** Gap junction-mediated intercellular biochemical coupling in cochlear supporting cells is required for normal cochlear functions. *Proc Natl Acad Sci USA* 102: 15201–15206, 2005.
 46. **Zhao HB, Kikuchi T, Ngezahayo A, White TW.** Gap junctions and cochlear homeostasis. *J Membr Biol* 209: 177–186, 2006.